

Long-Lived Spin-Polarized Intermolecular Exciplex States in Thermally Activated Delayed Fluorescence-Based Organic Light-Emitting Diodes

Sebastian Weissenseel, Andreas Gottscholl, Rebecca Bönnighausen,
Vladimir Dyakonov, Andreas Sperlich*

Experimental Physics 6 and Würzburg-Dresden Cluster of Excellence ct.qmat, Julius Maximilian University of Würzburg, 97074 Würzburg, Germany

Abstract

Spin-spin interactions in organic light-emitting diodes (OLEDs) based on thermally activated delayed fluorescence (TADF) are important because radiative recombination is largely determined by triplet-to-singlet conversion, also called reverse intersystem crossing (RISC). Less obvious is the fact that the non-emissive triplet states are spin-polarized, e.g., by charge injection, and spin-selection rules prevent part of the triplet population from RISC. To explore the relationship between these two processes, we apply a two-frequency spin-resonance technique, which is essentially spectral hole burning, that directly probes electroluminescence. This allows us not only to independently confirm high spin-polarization, but also to distinguish between individual triplet exciplex states distributed in the OLED emissive layer. These states can be decoupled from the heterogeneous nuclear environment as a source of spin dephasing and can even be coherently manipulated on a spin-spin relaxation time scale T_2^* of 30 ns. Furthermore, we obtain the characteristic spin-lattice relaxation time T_1 of the triplet exciplex in the range of 50 μ s, which is longer than the RISC time. We conclude that long spin relaxation time rather than RISC is an efficiency-limiting step for intermolecular donor:acceptor systems. Finding TADF emitters with faster spin relaxation will benefit this type of TADF OLEDs.

Introduction

The technological development of organic light-emitting diodes (OLEDs) has undergone remarkable progress and the market share of OLED displays in television and smart device applications is growing significantly. Initially started with fluorescence-based emitters with a maximum internal quantum efficiency (IQE) of 25%, phosphorescent molecular emitters with enhanced spin-orbit coupling (SOC) enabled much higher device efficiencies through singlet-to-triplet intersystem crossing (ISC) (1–4). In order to achieve 100% IQE with molecular systems which do not contain heavy elements, the concept of thermally activated delayed fluorescence (TADF), originally known as E-type delayed fluorescence (5–8) has been successfully employed in devices and substantially impacted OLED development over the last decade (9–11). In the TADF or E-type delayed fluorescence process, the first excited singlet state is populated by a thermally activated transition from the first excited triplet state. The mechanism for harvesting non-radiative triplet states is described as reverse intersystem crossing (RISC) (12–16). Upon injection of electrons and holes from the contacts into the active layer, which consists of donor and acceptor molecules, intermolecular exciplex states are formed. In general, such Coulomb-bound quasiparticles can be either in the singlet ($S = 0$) or triplet ($S = 1$) state, where the latter should in principle be accurately described by the spin Hamiltonian and, very importantly, can also be selectively controlled, e.g., by an external magnetic field or electron paramagnetic resonance (EPR), to track the population transfer to the singlet manifold. Of the two possible spin orientations of the exciplex state, EPR can selectively influence (flip) only triplet states, while the effect of the spin-flip is observed in a change of a radiative singlet exciplex state recombination. The missing puzzle piece is the connection between these two spin states, as RISC is a first-order spin-forbidden process (17–20). However, it can be thermally activated, i.e. as a result of electron-phonon interactions or through the admixture of other spin states, which, for example, enhance spin-orbit coupling, through a Δg -mechanism (21–23), or due to hyperfine interaction with paramagnetic nuclei (protons, nitrogen etc.). In a spin resonance experiment, microwaves with a properly chosen energy (frequency) flip the spin orientation and connect the $m_s = \pm 1$ and $m_s = 0$ substates of a triplet exciplex, which in turn facilitates population transfer to an emissive singlet exciplex final state.

However, the underlying spin physics is quite complex as the spin-spin interactions in such electron-hole pairs depend strongly on the molecular environment, as well as on the details of how these excited states are created, e.g., optically excited or by injection from electrodes. (24, 25). Further, the strength of the spin-spin interaction determines the energy gap between the states $m_s = 0$ and $m_s = \pm 1$, the so-called zero-field splitting (ZFS), and in practice is given by the spatial distance. As expected, the radii of the e-h pairs in the disordered organic systems have a very broad distribution. Thus, the sought-after spectroscopic precision of EPR methods for manipulating spin states is compromised by the fact that the excited spin-pairs (charge transfer (CT) states, exciplexes) are broadly distributed in a heterogeneous mixture of molecules, leading to inhomogeneously broadened envelopes instead of

* sperlich@physik.uni-wuerzburg.de

discrete resonance transitions (spin flips) and complicating access to the parameters of the spin Hamiltonian.

Here, we analyze the role of spin-spin interactions in the electroluminescence (EL) emission of an OLED using the method of EL detected magnetic resonance (ELDMMR). Most importantly, we were able to disentangle the complexity associated with a broad distribution of spin pairs and propose an original technique to select sub-ensembles of e-h pairs and reconstruct the details of the inhomogeneously broadened ELDMMR envelope in this way. For this purpose, a two-frequency hole burning experiment is used, which pumps and saturates the spin system at a fixed frequency during the second probe frequency sweep (26–29). Remarkably, this pump-probe method not only allows the separation and addressing of individual spin packets in the inhomogeneously broadened ELDMMR spectrum, but also the observation of coherent population oscillations (CPO), which are observed as spikes with a very narrow linewidth (26–35). The hole burning effect is caused by decoupling of the triplet exciplex spin state from the heterogeneous molecular environment, while the CPO can be described as a two-level quantum system oscillating with the beat frequency between pump and probe. Remarkably, the observation of CPO implies highly spin-polarized exciplex triplet states, which are not at all expected in an electrically driven OLED, where injected charge carriers are generally not spin-correlated.

Spin-Spin Interactions in OLEDs

The results presented in this work were obtained on OLEDs based on the donor:acceptor system m-MTDATA:BPhen (4,4',4''-tris[phenyl(m-tolyl)amino]triphenylamine: 4,7 diphenyl-1,10-phenanthroline) in a device configuration of PEDOT:PSS (40 nm) / m-MTDATA (30 nm) / m-MTDATA : BPhen (70 nm, 1:1 ratio) / BPhen (30 nm) / Ca (5 nm) / Al (120 nm), as shown in **Figure 1a**. With the pure m-MTDATA and BPhen layers as hole and electron transport layers, PEDOT:PSS (poly(3,4-ethylenedioxythiophene) poly(styrenesulfonate)) as hole injection layer and a mixed layer of m-MTDATA and BPhen as emission layer. Typical *j*-V-EL and external quantum efficiency (EQE) curves are shown in Supporting Figure S1. The photoluminescence (PL) spectra of the pure materials are shown in Figure 1b. The EL spectrum of the device made from the mixed layer is clearly red-shifted and much broader compared to the emission spectra of the pristine molecules. The former is due to the formation of a bound exciplex state at the interface of the two molecules, with the electron localized at the lowest unoccupied molecular orbital (LUMO) of the acceptor BPhen and the hole localized at the highest occupied molecular orbital (HOMO) of the donor m-MTDATA, as schematically shown in the inset of Figure 1b (36–39). The much larger width is probably due to the broad energetic distribution of the emitting states, which we address below.

The electron and the hole both possess a spin of $S = \frac{1}{2}$. If these particles form a bound exciton or an exciplex (which we consider equivalent to a CT state), the total spin will be either $S = 0$ or $S = 1$. The Hamilton operator describing the triplet state is according to (40):

$$\mathcal{H} = \underbrace{-S_a^T J S_b}_{\text{exchange}} + \underbrace{g\mu_B \mathbf{S} \vec{B}}_{e\text{-Zeeman}} + \underbrace{\mathbf{S}^T \mathbf{D} \mathbf{S}}_{\text{ZFS}} + \underbrace{\mathbf{S}^T \mathbf{A} \mathbf{I}}_{\text{HFI}} \quad (1)$$

The first interaction term describes the exchange interaction of the two spins S_a, S_b through the orbital overlap of their wave functions, where the exchange integral J determines the energy gap ΔE_{ST} between singlet and triplet energy levels. The second term is the electron-Zeeman interaction with the static external magnetic field B , the Landé factor g , the Bohr magneton μ_B and the spin operator \mathbf{S} . The third and fourth terms describe spin-spin interactions: the electron-spin zero-field splitting (ZFS) and the electron-nuclear hyperfine interaction (HFI), with their respective tensors \mathbf{D} and \mathbf{A} . Quadrupole interaction and nuclear Zeeman splitting are neglected in this work because their contribution is negligible. A schematic representation of ZFS and broadening due to HFI is shown in Figure 1d. The $m_s = 0$ and $m_s = \pm 1$ triplet states are split by the ZFS parameter D (in frequency units) (41):

$$D/h = -\frac{\mu_0 \mu_B^2}{4\pi h} \frac{g_a g_b}{r_{ab}^3} (3\cos^2\theta - 1) \quad (2)$$

Here, μ_0 is the vacuum permeability, g_a and g_b are the Landé factors for spins a and b , θ is the angle between the direction of the magnetic field and the radius vector r_{ab} connecting the two spins. The HFI term is given by the interaction of the exciplex triplet with surrounding paramagnetic nuclei represented by the nuclear spin operator I . This leads to a further splitting of the $m_s = \pm 1$ sub-levels, where each nucleus contributes with $A_{0,i}$ and the HFI term in Equation 1 is extended by the summation over all nuclei. The total number N_{tot} of HFI-sub-levels for i non-equivalent nuclei is then given by $N_{\text{tot}} = (2I+1)^i$. For i equivalent nuclei several HFI-levels degenerate and the total number is given by $N_{\text{eq}} = (2i+1)$ (42).

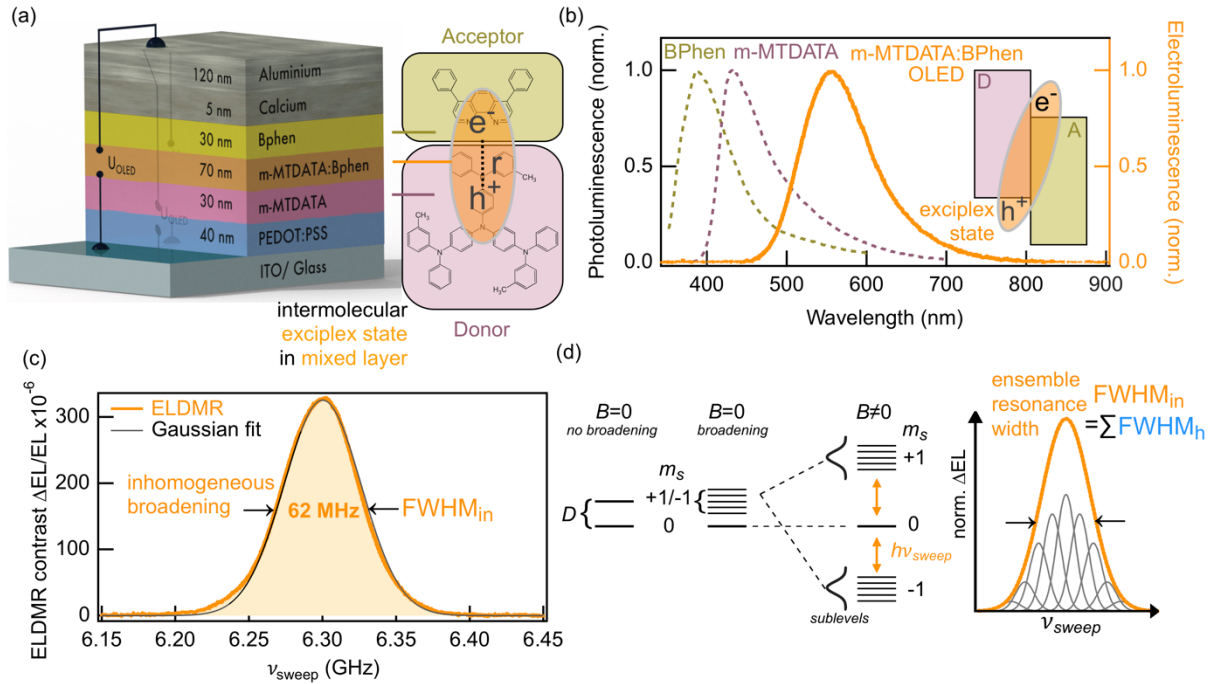


Figure 1. (a) Schematic of the m-MTDATA:BPhen OLED architecture. (b) Photoluminescence spectra of pure materials (left axis, dashed lines) and electroluminescence spectrum of an OLED device (right axis, solid orange line). The inset shows a bound exciplex state formed at the donor:acceptor interface. (c) Electroluminescence detected magnetic resonance (ELDMR) spectrum (orange line) of the m-MTDATA:BPhen OLED in a magnetic field of $B = 225$ mT and a Gaussian fit (black line) with FWHM of 62 MHz. (d) Triplet sub-levels with zero-field splitting D may exhibit broadening due to HFI. The sub-levels split in an external magnetic field and under resonant microwave irradiation with frequency ν_{sweep} , ΔEL is detected, which, as we will show later, is the envelope of the sum of homogeneous sub-spectra.

In conventional EPR, the external magnetic field is swept at a fixed microwave frequency, resulting in microwave absorption and spin-flip in the sample if the resonance criteria are met. For the ELDMR method used in this work, we couple an OLED to a stripline circuit that serves as an antenna for the frequency-swept microwaves at a fixed magnetic field. The strength of the effect is evaluated by the ELDMR contrast $\Delta\text{EL}/\text{EL}$. A detailed description of ELDMR can be found in previous publications (24, 25), where also the singlet-triplet energy gap $\Delta E_{ST} = 58$ meV was estimated for the MTDATA:BPhen blends, which is by far the largest energy contribution among the spin-spin interaction terms in Equation 1. An example ELDMR spectrum of an m-MTDATA:BPhen OLED device at $T = 220$ K is shown in Figure 1c, with the microwave frequency ν_{sweep} swept from 6.15 GHz to 6.45 GHz at fixed magnetic field $B = 225$ mT. The spectrum exhibits a featureless shape, which can be fitted with a Gaussian with a full width at half maximum (FWHM) of 62 MHz. This indicates that the ELDMR spectrum is inhomogeneously broadened. The working hypothesis that we verify in the following is that we are dealing with an ensemble of triplet states with different spin-spin interaction parameters and thus transition frequencies, showing up themselves as a featureless envelope, as schematically shown in Figure 1d. With knowledge of the details of the broadening of the ELDMR spectrum, e.g., due to the distribution of the spin-spin interaction, the broadening of the EL spectrum can also be better understood and potentially eliminated once it is assigned to a controllable structural or morphological parameter.

Hole Burning Spectroscopy

To explore the origin of spectral broadening, we apply a two-frequency ELDMR technique realized by introducing a second frequency (ν_{pump}) fixed within the ELDMR spectrum while simultaneously sweeping the frequency ν_{sweep} during the measurement, as schematically shown in Figure 2a. As illustrated, a dip occurs when a sufficiently high-power pump microwave field saturates a transition between triplet spin sub-levels (see Figures S2, S3). The width of the dip is associated to the energetic span of the sub-levels in the energy diagram (Figure 2a) (26, 27, 30–35). In Figure 2b, a continuous wave ELDMR spectrum is shown (orange curve). Applying the second microwave frequency results in a dip at the position of the applied pump frequency of $\nu_{\text{pump}} = 6.3$ GHz (Figure 2b, blue curve). This so-called "hole burning" technique is widely used in optical absorption and fluorescence spectroscopy, as well as in spin resonance, but it has never been reported for ELDMR (28, 29, 43–45).

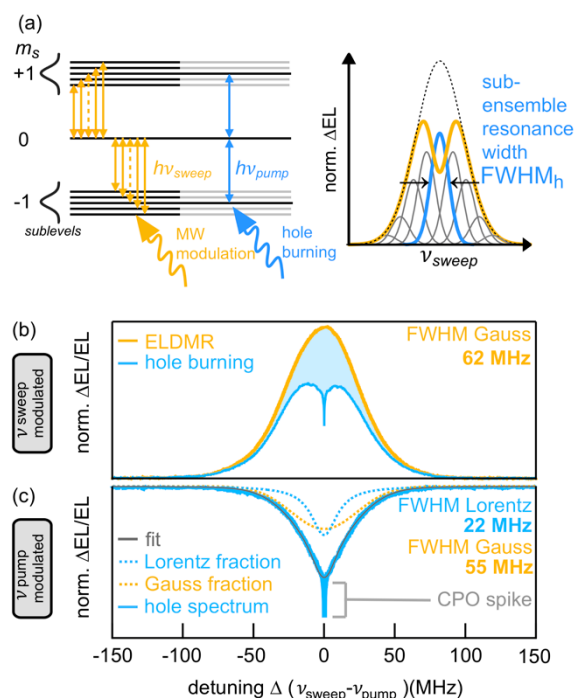


Figure 2. ELDMR hole burning. (a) Schematic of the energetically broadened triplet sub-levels with resonance transitions induced by a variable (orange arrows) and fixed microwave frequency (blue arrows), and hole burning in an inhomogeneously broadened ensemble. (b) ELDMR spectrum (orange) and hole burning spectrum (blue) of m-MTDATA:BPhen for a frequency sweep of ± 150 MHz around $\nu_{\text{pump}} = 6.3$ GHz. The sweep frequency ν_{sweep} is modulated “on-off” for lock-in detection and the pump frequency ν_{pump} is kept in continuous wave mode. (c) Directly measured hole spectrum by modulating the fixed frequency (ν_{pump}) instead of the sweep frequency (ν_{probe}). The signal consists of a broad Gaussian background (FWHM of 55 MHz), a narrower Lorentzian peak (FWHM of 22 MHz), and a very narrow spike in the center (FWHM of 12 kHz). The fitting curve (black) is a superposition of a Gaussian (dotted orange) and a Lorentzian (dotted blue) contribution.

To directly unveil the shape of the "spectral hole" shown in Figure 2b, we now modulate the pump frequency. The resulting spectrum in Figure 2c has a distinct, broad shape with a narrow spike on top. The latter is assigned to CPO, whose origin will be discussed in detail later. The broad spectrum can be perfectly fitted by the sum of Gauss and Lorentz functions with FWHM linewidths of 55 MHz and 22 MHz, respectively – represented by the dotted lines in Figure 2c. Note that the "hole" spectral shape is independent of which of the two frequencies is on/off modulated, ν_{sweep} or ν_{pump} , but since the pump frequency directly saturates a particular transition in the triplet sub-ensemble, we have used it in Figure 2c and in the following.

To investigate the structure of the hole in more detail, we varied the pump frequency, as shown in **Figure 3**. It shows a two-dimensional map in which the hole spectra are recorded as a function of ν_{pump} and ν_{sweep} in a frequency range from 6.25 GHz to 6.35 GHz. The analysis clearly shows that the hole spectrum can be decomposed into two contributions, Gaussian and Lorentzian. Furthermore, the Lorentzian contribution can be moved through the entire ELDMR spectrum, while the Gaussian contribution remains constant. The individual fits to the hole spectra are shown in Figure S4. Figure 3b exemplarily shows the corresponding cuts for three pump frequencies. When the pump frequency is shifted from the central $\nu_{\text{pump}} = 6.3$ GHz to the side flanks, the holes become asymmetric, also indicating that the Gaussian background does not depend on ν_{pump} (Figure 3a, bottom left), but the Lorentzian line does (Figure 3a, bottom right). However, the width of the Gaussian background (55 MHz) is slightly less than the total measured ELDMR linewidth, which is 62 MHz, which could indicate a different origin. To verify this, we evaluated the two contributions separately and used them to reconstruct the experimental ELDMR spectrum. The individual linewidths for Gaussian and Lorentzian contributions are shown in Figure 3c. While the Lorentz linewidth remains constant at 22 MHz and does not change with ν_{pump} , the Gauss linewidth varies between 50 and 62 MHz in the applied range of pump frequencies. As shown in Figure 3d, we can perfectly reconstruct the ELDMR spectrum by summing all contributions

in the pump frequency range studied. This illustrates that the inhomogeneously broadened spectrum is the envelope of superimposed sub-spectra, that can be revealed by hole burning spectroscopy.

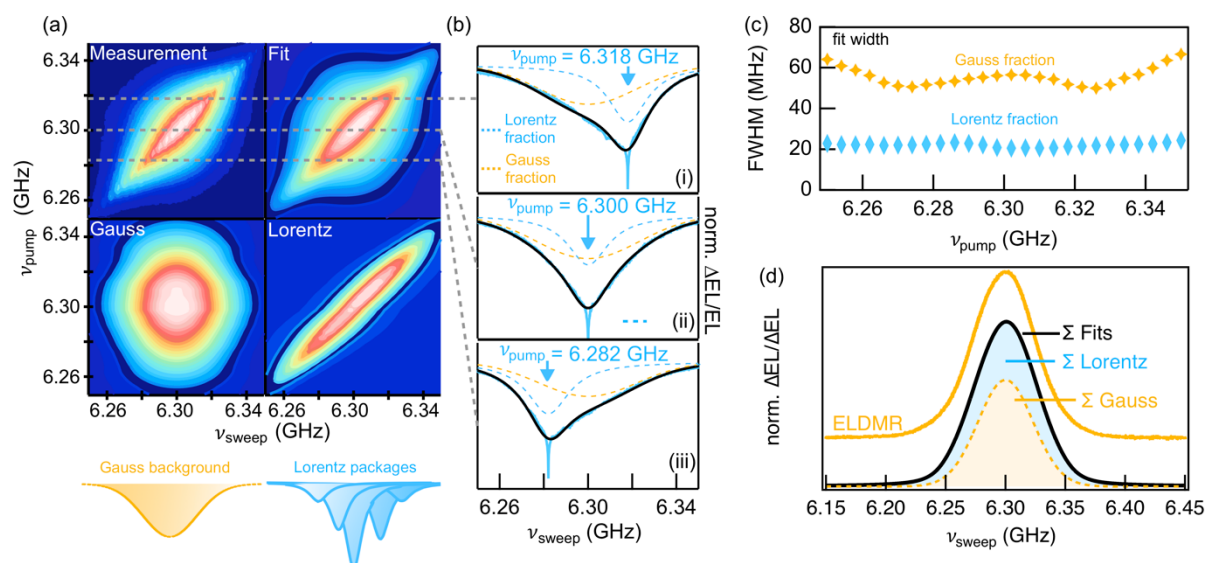


Figure 3. Spectral analysis of the hole by varying the pump frequency ν_{pump} . (a) Color map of the hole spectrum as a function of ν_{sweep} and ν_{pump} . The fit map is the sum of the Gauss and Lorentz maps. The Gaussian contribution is centered at $\nu_{\text{sweep}} = 6.30$ GHz, while the Lorentzian varies with ν_{pump} , as shown schematically at the bottom. (b) Hole contributions as a function of ν_{pump} . While the Lorentz line shifts with pump frequency, the Gaussian contribution remains fixed. (c) FWHM for Gauss and Lorentz contributions as a function of ν_{pump} . (d) Reconstruction of the ELDMR signal from the Lorentzian and Gaussian contributions. The sum of all fits has the same linewidth and shape as the ELDMR spectrum.

The fitted intensities of the Lorentz fraction can further be used to determine the dipolar interaction D of electron and hole within the exciplex as shown in Figure S5b of the Supporting Information. The fitted intensities reveal the underlying triplet spectrum without the Gaussian background and this spectrum can be simulated with $D = 50 \pm 5$ MHz. From D we can also estimate the e-h separation within the exciplex (41) to be $r_{e-h} [\text{nm}] = \sqrt[3]{78.05/D [\text{MHz}]} \text{ nm} = 1.1 \text{ nm} - 1.2 \text{ nm}$, i.e., matching the expected delocalization over neighboring molecules. The coupling distance of emissive exciplex states is therefore quite uniform.

This analysis shows that the inhomogeneous broadening of the ELDMR spectrum is not due to a broad distribution of triplet exciplex states with different e-h separations and thus dipolar interactions. Instead, we propose spectral diffusion of overlapping spin packets as a reason for unresolved HFI, which has also been reported for other spin systems, e.g., for color centers in diamonds (27) and which we discuss in the following. The same process is responsible for the inhomogeneous broadening and thus for the Gaussian background.

Inhomogeneous Spectral Broadening by Unresolved HFI

With the hole burning method we revealed an underlying homogeneous linewidth and identified an additional inhomogeneous Gaussian broadening. For this broadening we can exclude effects due to high microwave power and the Δg -mechanism as shown in detail in the Supporting Information. In the following, we will show that it can be assigned to unresolved HFI with paramagnetic nuclei in the molecules. For m-MTDATA:BPhen this includes $i_H = 64$ ^1H protons with a nuclear spin of $I = 1/2$ and $i_N = 6$ ^{14}N nitrogen nuclei with $I = 1$, while other paramagnetic isotopes have negligible abundance. The isotropic hyperfine coupling constant A depends on the electron-nuclei wavefunction overlap – the Fermi contact interaction (46). In organic molecular systems, e-h wavefunctions delocalize, involving more interacting nuclei, but decreasing the average HFI (motional narrowing) (47–49). Electron-proton HFI A_H is usually weak and unresolved, leading to inhomogeneous broadening (50–54). For exciplexes in a similar TADF system, $A_{H,max} < 5.5$ MHz was determined as an upper limit (55), whereas for charge-separated states in polymer:fullerene blends, $A_{H,max}$ of 2 – 3 MHz (50) or 4 – 5 MHz (51) was estimated. Considering the large molecular extent of m-MTDATA:BPhen and that protons at the edges of molecules are not part of the conjugated electron system, we can expect $A_H < 2$ MHz.

HFI with a discrete number ($i_N = 4$) of ^{14}N nuclei directly incorporated in the conjugated system of triphenylamine-derivatives has been determined to $A_N = 2.5 - 3.8$ MHz (56). We performed exemplary HFI simulations (81) of the exciplex triplet with $i_N = 6$ ^{14}N as presented in the Supporting Information and estimate $A_N < 2$ MHz.

The unresolved and weak HFI in m-MTDATA:BPhen can explain the inhomogeneous linewidth broadening. More intriguing, however, is the fact that $A_{H,N} < 2$ MHz is considerably smaller than the ZFS $D < 50$ MHz. This suggests that HFI is too weak to mediate RISC rates as the exciplex triplet is decoupled from the nuclear spin bath by the stronger ZFS D .

Coherent Population Oscillations of Spin-Polarized Exciplex States

In a hole burning experiment, we apply two microwave fields to the spin system. From a classical viewpoint, when two electromagnetic waves with nearby frequencies interfere, a beat oscillation of intensity occurs with the beat frequency $\Delta\nu = \nu_{\text{sweep}} - \nu_{\text{pump}}$, where $\Delta\nu$ is the detuning between pump and probe frequencies (see Figure S9). While the application of a single microwave resonance frequency tends to equilibrate the population of spin sub-levels, the simultaneous application of two frequencies to a highly spin polarized system can cause the triplet population to oscillate, especially when the beat frequency is in the range of or lower than the inverse spin relaxation time of the spin system. This CPO effect has been reported for various inorganic spin systems in the past (27, 44, 57, 58) and is also known from laser spectroscopy of two-level systems (59). In a lock-in detected ELDMMR experiment, as in ours, these oscillations are time-averaged. This leads to a beat frequency $\Delta\nu$ -dependent depth of the burned spectral hole. Spin relaxation is mediated by a longitudinal spin-lattice relaxation time T_1 and a transverse dephasing time T_2^* and they will determine the eigenfrequencies of the spin state. In the case of a forced oscillation with the variable beat frequency, the "hole" depth will be affected. In a continuous detuning scan, the beat frequency is varied from a few Hz to MHz, and we observe such a very narrow spike on the top of the hole, as shown in **Figure 4**. The homogeneous linewidth $\text{FWHM}_h = 22$ MHz allows to estimate a lower limit for the dephasing time $T_2^* > 2/(\pi \cdot \text{FWHM}_h) = 30$ ns, while the width of the spike corresponds to the spin-lattice relaxation time. The dephasing time agrees well with estimated from pulsed Rabi experiments on similar OLED systems (55, 60).

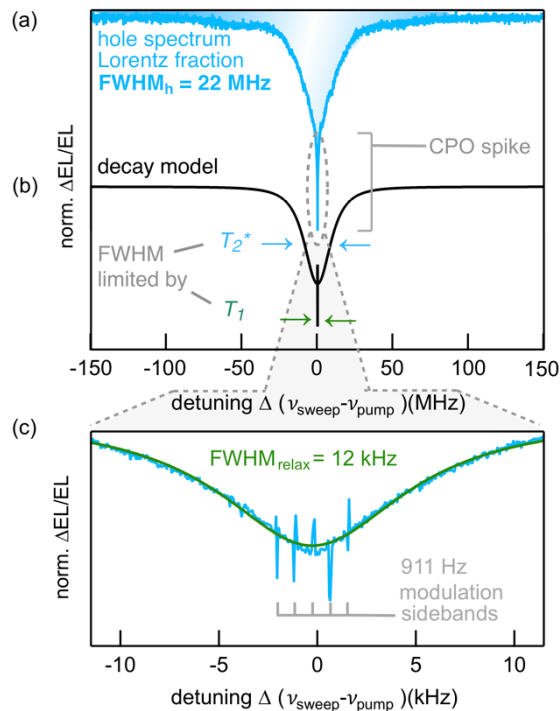


Figure 4. Coherent Population Oscillations (CPO). (a) Lorentz fraction of the hole spectrum with CPO spike. We subtracted the Gaussian background (see Fig. 3a) for clarity. (b) FFT of the decay model in Equation 3. The FWHM is limited by dephasing time T_2^* and spin-lattice relaxation time T_1 (c) Zoomed-in measurement of the hole spectrum. The spike can be described by one Lorentzian, which results from CPO between triplet levels due to microwave beating between ν_{sweep} and ν_{pump} .

When changing from frequency to time domain, one can assume a simple decay model. The net magnetization of a sub-ensemble of $S = 1$ states formed at $t = 0$ decays exponentially with the time

constants T_2^* and T_1 . In an external magnetic field, it is also undergoing precession with the Larmor frequency $\nu_L = \omega_L/2\pi$. Thus, we can write for the intensity of net magnetization of a sub-ensemble:

$$I(t) = \left[A \cdot \exp\left(-\frac{t}{T_2^*}\right) + B \cdot \exp\left(-\frac{t}{T_1}\right) \right] \cdot \sin(\omega_L \cdot t), \quad (3)$$

with amplitudes A and B , respectively. The fast Fourier transform (FFT) of this equation is shown in Figure 4b. The fast decay due to T_2^* gives a broad signal, while the FFT of the long decay with T_1 reproduces the spike. By zooming in on the spike in Figure 4a, it turns out that the shape is more complex and cannot be perfectly fitted with a single Lorentzian function. The shape can however be fully reproduced by applying a modified three-level model of (27). This is possibly due to inhomogeneous broadening of the triplet sub-levels involved, but the issue cannot be fully elucidated. For further details, we refer to the Supporting Information. We can nevertheless estimate $\text{FWHM}_{\text{relax}} = 12$ kHz for the narrowest contribution as shown in Figure 4c with which we can estimate an upper limit of the spin-lattice relaxation time $T_1 < 2/(\pi \cdot \text{FWHM}_{\text{relax}}) = 50$ μs . These measurements were performed at an experimental temperature of $T = 220$ K. In between 290 K and 160 K (Figure S12) we observed that T_1 is not very temperature-sensitive as it increases from 50 μs to 70 μs when cooling. Interestingly, modulation sidebands appear due to on-off modulation of the pump frequency with $\nu_{\text{mod}} = 911$ Hz, which rules out the possibility that on-off modulation effects are responsible for contributions to CPO in the kHz to MHz range. We also exclude ν_{mod} to influence the determined T_1 time by measuring with different modulation frequencies (see Figure S13).

Discussion

Interplay Between RISC and Spin Relaxation of Triplet Exciplex States

In the following, we discuss the role of the determined spin-spin interactions and spin relaxation times in comparison with RISC time constants. Interaction strengths (A , D , $g\mu_B B$) and FWHM linewidths are given in frequency units, while time constants are always given in time units and not as rates.

The observation of CPO in the EL of working OLEDs is striking as it proves that the emitting exciplex states are in fact highly spin-polarized. This is a remarkable finding as injected charge carriers are generally not spin-correlated and upon recombination at the donor:acceptor interface will populate the exciplex singlet and triplet $m_s = 0, \pm 1$ sub-levels evenly. Singlet states recombine on a nanosecond time scale, leaving the triplets to undergo RISC to facilitate delayed fluorescence. The fact that we observe spin-polarized exciplexes in electrically driven devices unambiguously teaches us that recombination of triplet exciplexes is highly spin-dependent with unequal RISC rates for the $m_s = 0, \pm 1$ sub-levels. The selection rules ($\Delta S = \pm 1$, $\Delta m_s = 0$) for transitions between singlet ($S = 0$, $m_s = 0$) and triplet ($S = 1$, $m_s = 0, \pm 1$) exciplex states would favor faster depletion of $m_s = 0$ triplet exciplexes and can thus be responsible (compare Figure S6).

Spin polarization decays with the spin-lattice relaxation time $T_1 < 50$ μs , which by far exceeds RISC on the timescale of 30 – 220 ns for this material system (25). Similar T_1 times around 30 μs were reported for other OLED systems and even organic solar cells probed by electrically and optically detected magnetic resonance (EDMR, ODMR) (61–64). A long spin relaxation time is hereby typical for organic materials with weak HFI and significant ZFS as this decouples the electron spin system from relaxation caused by the nuclear spin bath. It should be noted that while the presented experiments are carried out in an external magnetic field that results in a triplet state Zeeman splitting of $g\mu_B B = 6.3$ GHz, i.e., much larger than ZFS and HFI, the spin polarization mechanism will be identical even without applied magnetic field. The ZFS of $D = 50$ MHz is sufficiently large to decouple the electron spin system from the nuclear spin bath in zero magnetic field, preserving a long T_1 time. RISC time constants for other donor:acceptor exciplex (9, 65–68) and molecular TADF materials (69–72) were reported around 0.5 μs – 2 μs (67–71) or up to 30 μs (65, 66, 72) – always being shorter, or even significantly shorter than T_1 . This imbalance between RISC and T_1 time constants by up to more than an order of magnitude leads to spin polarization between $m_s = 0, \pm 1$ levels and we can thus assume it to be in the order of or greater than 90% ($= 1 - \frac{T_{\text{RISC}}}{T_1}$). Therefore, in the majority of TADF OLEDs, a strong spin polarization is expected, which unnecessarily prolongs the lifetime of the excited states. This may ultimately limit quantum efficiencies, especially at high OLED current densities and lead to efficiency roll-off that is usually ascribed to triplet-triplet and triplet-charge annihilation (10, 12, 66). This finding strongly implies that spin polarization of triplets must be suppressed by a mechanism to accelerate spin relaxation. T_1 can be significantly shortened by molecular curvature-enhanced spin-orbit coupling (SOC) as has been

shown theoretically (73) and experimentally (74, 75). Additionally, T_1 scales with the Δg -mechanism as $T_1 \sim (\Delta g)^{-2}$ (76). Both mechanisms can be employed for the design of next-generation TADF systems.

In contrast to the long T_1 time, the spin dephasing time $T_2^* > 30$ ns is exceptionally short and actually limits the homogeneous linewidth $\text{FWHM}_h = 22$ MHz. Such fast dephasing is often mediated by interaction with multiple, almost equally coupled nuclei (77) as in our case with nitrogen nuclei and protons. RISC is on the same timescale or even considerably longer than T_2^* which means that spins will dephase quickly and RISC is not affected by a short T_2^* . Consequently, the ensemble of exciplexes in an OLED is highly incoherent, i.e., T_2^* is short enough to not affect the operation of the OLED at all.

Comparison with other Donor:Acceptor Systems

Finally, it is intriguing to compare the exciplex states in intermolecular TADF emitters studied here with excited states in other material systems, such as CT states in intramolecular TADF emitters and polymer:fullerene blends used in organic photovoltaics (OPV). (While exciplex and CT states are essentially the same kind of species.) Both, exciplex- and CT-based TADF emitter systems exhibit high internal quantum efficiencies and have singlet-triplet gaps ΔE_{ST} in the range of thermal energy. However, dipolar interactions differ by at least an order of magnitude, with $D > 500$ MHz determined for intramolecular TADF emitters (18, 20), clearly indicating their stronger localization compared to the system studied here. In contrast, OPV CT states have an order of magnitude smaller dipolar interaction of $D < 5$ MHz and $\Delta E_{ST} < 5$ MHz, which corresponds to 20 neV, i.e., over six orders of magnitude smaller than for TADF (78). This corresponds to a much wider excited state delocalization and a weaker oscillator strength. Hence, it is not surprising that OPV CT states exhibit very low EL quantum efficiency in the order of 10^{-6} (79). We conclude, the m-MTDATA:BPhen exciplex emitter with $D = 50 \pm 5$ MHz and a singlet-triplet gap of $\Delta E_{ST} = 58$ meV (24, 25) is an intermediate case, between highly emissive intramolecular TADF and poorly-emissive OPV CT states, revealing large or nearly zero dipolar interactions, respectively.

Conclusion

In conclusion, we have experimentally shown that electrical injection of charge carriers into OLEDs based on the TADF system m-MTDATA:BPhen results in the buildup of a spin-polarized triplet exciplex population with long spin-lattice relaxation time. This phenomenon is initially due to spin-statistically injected charges in the devices but can be considered detrimental to OLED efficiency since these exciplex species are not undergoing RISC. The observation was made possible by implementing a novel two-frequency spin-resonance spectroscopy based on so-called "hole burning" by direct monitoring of the electroluminescence intensity. We used it to observe coherent population oscillations that exhibit an electroluminescence spike of extremely narrow width, from which we not only prove >90% spin-polarization itself, but also estimate the spin-lattice relaxation time of 50 μ s, which is thus longer than the RISC time constants in this and similar TADF systems. Furthermore, our spin resonance protocol provided insights into the inhomogeneously broadened triplet exciplex spectra consisting of individual sub-ensembles or "spectral holes" with a characteristic zero-field splitting parameter $D = 50 \pm 5$ MHz, indicating exciplex states of 1.1 nm – 1.2 nm extent, i.e., over adjacent donor:acceptor molecular pairs. The broadening is the result of the disordered nature of the molecular blends, but it can be also quantitatively understood as the result of unresolved hyperfine interactions with the surrounding protons and the nitrogen nuclei, and we provide an estimate of the strength of an averaged nuclear field that is in the range of 2 MHz. The fact that the spin relaxation time is much longer than the RISC time clearly implies that the type of TADF OLEDs studied here is efficiency-limited due to the spin polarization, which needs to be suppressed by a mechanism to accelerate the relaxation, such as spin-orbit coupling. Our findings further put the commonly targeted small singlet-triplet gap and thus high RISC rate into perspective.

Experimental Section

Device Fabrication

For OLED devices ITO-covered glass substrates (Vision-Tek Systems) were used. The hole injection layer PEDOT:PSS (4083Ai, Heraeus) was spin coated at 3000 rpm, resulting in a 40 nm thick film. It is thermally annealed for 10 min at 130°C. Remaining layers are evaporated under vacuum. The hole transport layer (HTL, m-MTDATA) and electron transport layer (ETL, BPhen) have a thickness of 30 nm. In-between, a 70 nm mixed layer of both materials is deposited as emission layer (EML). A top electrode consisting of calcium (5 nm) and aluminum (120 nm) was used, resulting in an active area of 3 mm².

Device Characterization

J-*V*-EL and EQE characteristics were measured with a parameter analyzer (Agilent 4155C) and a silicon photo detector placed on top of the OLED.

Magnetic Resonance

For ELDMR measurements, we used a modified EPR spectrometer (Bruker ESP300) with a nitrogen flow cryostat (Oxford 935). The temperature for all measurements was $T = 220$ K, except for Figure S12. The microwaves are generated with a signal generator (Anritsu MG3694C). The output power for all measurements was set to 0 dBm, amplified by a 3 W amplifier (Mini-Circuits ZVW-3W-183+). The OLED device was placed on top of a microwave strip-line to enable spin control in the emission layer. A source measure unit (Keithley 237) drives the OLED in constant current mode ($j = 1.6$ mA/cm²) and the EL is detected by a photodiode (Hamamatsu, S2387-66R) and amplified by a current-voltage amplifier (Femto DLPCA-200). The change of EL upon resonant microwaves, ΔEL , was detected via a lock-in-amplifier (SR7265).

Hole Burning Spectroscopy

In a hole burning experiment, the pump microwave generator (Synth HD, Windfreak) was amplified by a secondary 3W amplifier. The outputs of both amplifiers are merged by a high-power combiner (Mini-Circuits ZN2PD-183W-S+). Hole burning spectra are detected by modulation of the sweep microwave generator. Direct detection of hole spectra is realized by modulation of the pump generator.

Supporting Information is available.

Acknowledgements

S.W. acknowledges support by the German Research Foundation, DFG, within FOR1809 (DY18/12-2). A.G., V.D. and A.S. acknowledge financial support from the DFG through the Würzburg-Dresden Cluster of Excellence on Complexity and Topology in Quantum Matter – ct.qmat (EXC 2147, project-id 39085490). We thank Jeannine Grüne for fruitful discussions.

Competing Interests

The authors declare that they have no competing interests

Author Contributions

S.W., A.G. and A.S. designed the experiments that were performed by S.W. and R.B. Data analysis was performed by S.W., A.G. and A.S. The draft was written by S.W., V.D. and A.S., with all authors contributing in iterations. The project was supervised by V.D. and A.S.

Supplementary Materials

Device characteristics, spectral broadening mechanisms including CPO simulations, dependence of T_1 time on experimental conditions.

ORCID

Sebastian Weissenseel: [0000-0001-9811-1005](https://orcid.org/0000-0001-9811-1005)

Andreas Gottscholl: [0000-0002-9724-1657](https://orcid.org/0000-0002-9724-1657)

Vladimir Dyakonov: [0000-0001-8725-9573](https://orcid.org/0000-0001-8725-9573)

Andreas Sperlich: [0000-0002-0850-6757](https://orcid.org/0000-0002-0850-6757)

References

1. A. R. Brown, K. Pichler, N. C. Greenham, D. D. C. Bradley, R. H. Friend, A. B. Holmes, Optical spectroscopy of triplet excitons and charges excitations in PPV LEDs. *Chem. Phys. Lett.* **210**, 61–66 (1993).
2. V. Cleave, G. Yahioğlu, P. Le Barny, R. H. Friend, N. Tessler, Harvesting Singlet and Triplet Energy in Polymer LEDs. *Adv. Mater.* **11**, 285–288 (1999).
3. L. S. Swanson, J. Shinar, A. R. Brown, D. D. C. Bradley, R. H. Friend, P. L. Burn, A. Kraft, A. B. Holmes, Electroluminescence-detected magnetic-resonance study of poly(paraphenylenevinylene) (PPV)-based light-emitting diodes. *Phys. Rev. B.* **46**, 15072–15077 (1992).
4. B. Minaev, E. Jansson, H. Ågren, S. Schrader, Very high-efficiency green organic light-emitting devices based on electrophosphorescence. *Nat. Transit. orbitals J. Chem. Phys.* **125**, 164112 (2006).
5. S. Boudin, Phosphorescence des solutions glycériques d'éosine influence des iodures. *J. Chim. Phys.* **27**, 285–290 (1930).
6. C. A. Parker, C. G. Hatchard, Triplet-singlet emission in fluid solutions. Phosphorescence of eosin. *Trans. Faraday Soc.* **57**, 1894 (1961).
7. G. N. Lewis, D. Lipkin, Reversible photochemical processes in rigid media. a study of the

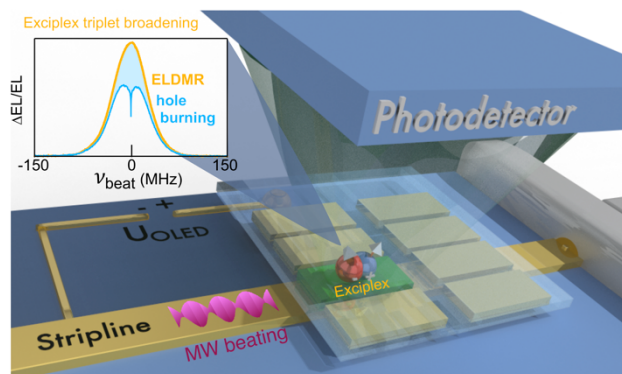
- phosphorescent state. *J. Am. Chem. Soc.* (1941), doi:10.1021/ja01856a043.
8. J. Saltiel, H. C. Curtis, L. Metts, J. W. Miley, J. Winterle, M. Wrighton, Delayed Fluorescence and Phosphorescence of Aromatic Ketones in Solution. *J. Am. Chem. Soc.* **92**, 410–411 (1970).
 9. K. Goushi, K. Yoshida, K. Sato, C. Adachi, Organic light-emitting diodes employing efficient reverse intersystem crossing for triplet-to-singlet state conversion. *Nat. Photonics.* **6**, 253–258 (2012).
 10. Q. Zhang, B. Li, S. Huang, H. Nomura, H. Tanaka, C. Adachi, Efficient blue organic light-emitting diodes employing thermally activated delayed fluorescence. *Nat. Photonics.* **8**, 326–332 (2014).
 11. H. Uoyama, K. Goushi, K. Shizu, H. Nomura, C. Adachi, Highly efficient organic light-emitting diodes from delayed fluorescence. *Nature.* **492**, 234–238 (2012).
 12. M. Y. Wong, E. Zysman-Colman, Purely Organic Thermally Activated Delayed Fluorescence Materials for Organic Light-Emitting Diodes. *Adv. Mater.* **29**, 1605444 (2017).
 13. Z. Yang, Z. Mao, Z. Xie, Y. Zhang, S. Liu, J. Zhao, J. Xu, Z. Chi, M. P. Aldred, Recent advances in organic thermally activated delayed fluorescence materials. *Chem. Soc. Rev.* **46**, 915–1016 (2017).
 14. Y. Im, M. Kim, Y. J. Cho, J.-A. Seo, K. S. Yook, J. Y. Lee, Molecular Design Strategy of Organic Thermally Activated Delayed Fluorescence Emitters. *Chem. Mater.* **29**, 1946–1963 (2017).
 15. Y. Liu, C. Li, Z. Ren, S. Yan, M. R. Bryce, All-organic thermally activated delayed fluorescence materials for organic light-emitting diodes. *Nat. Rev. Mater.* **3**, 18020 (2018).
 16. X. Cai, S. Su, Marching Toward Highly Efficient, Pure-Blue, and Stable Thermally Activated Delayed Fluorescent Organic Light-Emitting Diodes. *Adv. Funct. Mater.* **28**, 1802558 (2018).
 17. Y. Wang, K. Sahin-Tiras, N. J. Harmon, M. Wohlgenannt, M. E. Flatté, Immense Magnetic Response of Exciplex Light Emission due to Correlated Spin-Charge Dynamics. *Phys. Rev. X.* **6**, 011011 (2016).
 18. E. W. Evans, Y. Olivier, Y. Puttisong, W. K. Myers, T. J. H. Hele, S. M. Menke, T. H. Thomas, D. Credgington, D. Beljonne, R. H. Friend, N. C. Greenham, Vibrationally Assisted Intersystem Crossing in Benchmark Thermally Activated Delayed Fluorescence Molecules. *J. Phys. Chem. Lett.* **9**, 4053–4058 (2018).
 19. M. K. Etherington, N. A. Kukhta, H. F. Higginbotham, A. Danos, A. N. Bismillah, D. R. Graves, P. R. McGonigal, N. Haase, A. Morherr, A. S. Batsanov, C. Pflumm, V. Bhalla, M. R. Bryce, A. P. Monkman, Persistent Dimer Emission in Thermally Activated Delayed Fluorescence Materials. *J. Phys. Chem. C.* **123**, 11109–11117 (2019).
 20. T. Ogiwara, Y. Wakikawa, T. Ikoma, Mechanism of Intersystem Crossing of Thermally Activated Delayed Fluorescence Molecules. *J. Phys. Chem. A.* **119**, 3415–3418 (2015).
 21. M. Pope, C. E. Swenberg, *Electronic Processes in Organic Crystals and Polymers* (Electronic Processes in Organic Crystals and Polymers, 1999).
 22. U. E. Steiner, T. Ulrich, Magnetic field effects in chemical kinetics and related phenomena. *Chem. Rev.* **89**, 51–147 (1989).
 23. Z. V. Vardeny, *Organic Spintronics* (CRC Press, 2010; <https://www.taylorfrancis.com/books/9781439806579>).
 24. S. Väh, K. Tvingstedt, M. Auth, A. Sperlich, A. Dabuliene, J. V. Grazulevicius, P. Stakhira, V. Cherpak, V. Dyakonov, Direct Observation of Spin States Involved in Organic Electroluminescence Based on Thermally Activated Delayed Fluorescence. *Adv. Opt. Mater.* **5**, 1600926 (2017).
 25. N. Bunzmann, S. Weissenseel, L. Kudriashova, J. Gruene, B. Krugmann, J. V. Grazulevicius, A. Sperlich, V. Dyakonov, Optically and electrically excited intermediate electronic states in donor:acceptor based OLEDs. *Mater. Horizons.* **7**, 1126–1137 (2020).
 26. P. R. Moran, Electron Spin Double Resonance Studies of F- Centers in KCl. I. *Phys. Rev.* **135**, A247–A265 (1964).
 27. M. Mrozek, A. M. Wojciechowski, D. S. Rudnicki, J. Zachorowski, P. Kehayias, D. Budker, W. Gawlik, Coherent population oscillations with nitrogen-vacancy color centers in diamond. *Phys. Rev. B.* **94**, 1–11 (2016).
 28. V. A. Soltamov, C. Kasper, A. V. Poshakinskiy, A. N. Anisimov, E. N. Mokhov, A. Sperlich, S. A. Tarasenko, P. G. Baranov, G. V. Astakhov, V. Dyakonov, Excitation and coherent control of spin qubit modes in silicon carbide at room temperature. *Nat. Commun.* (2019), doi:10.1038/s41467-019-09429-x.
 29. A. Gottscholl, M. Diez, V. Soltamov, C. Kasper, A. Sperlich, M. Kianinia, C. Bradac, I. Aharonovich, V. Dyakonov, Room temperature coherent control of spin defects in hexagonal boron nitride. *Sci. Adv.* **7**, eabf3630 (2021).
 30. W. R. Bennett, Hole Burning Effects in a He-Ne Optical Maser. *Phys. Rev.* **126**, 580–593 (1962).
 31. H. A. R. El-Ella, A. Huck, U. L. Andersen, Continuous microwave hole burning and population oscillations in a diamond spin ensemble. *Phys. Rev. B.* **100**, 214407 (2019).

32. W. E. Moerner, Ed., *Persistent Spectral Hole-Burning: Science and Applications* (Springer Berlin Heidelberg, Berlin, Heidelberg, 1988; <http://link.springer.com/10.1007/978-3-642-83290-1>), vol. 44 of *Topics in Current Physics*.
33. M. Mrózek, D. Rudnicki, P. Kehayias, A. Jarmola, D. Budker, W. Gawlik, Longitudinal spin relaxation in nitrogen-vacancy ensembles in diamond. *EPJ Quantum Technol.* **2**, 22 (2015).
34. K. W. Roushlang, J. B. Alexander Ross, A. L. Kwiram, D. A. Deranleau, Triplet State of Tryptophan in Proteins: The Nature of the Optically Detected Magnetic Resonance Lines. *Biochemistry.* **17**, 1087–1092 (1978).
35. J. U. von Schütz, J. Zulich, A. H. Maki, Resolution of Tryptophan Phosphorescence from Multiple Sites in Proteins using Optical Detection of Magnetic Resonance. *J. Am. Chem. Soc.* **96**, 714–718 (1974).
36. K. Goushi, C. Adachi, Efficient organic light-emitting diodes through up-conversion from triplet to singlet excited states of exciplexes. *Appl. Phys. Lett.* **101**, 23306 (2012).
37. W. Y. Hung, G. C. Fang, Y. C. Chang, T. Y. Kuo, P. T. Chou, S. W. Lin, K. T. Wong, Highly efficient bilayer interface exciplex for yellow organic light-emitting diode. *ACS Appl. Mater. Interfaces.* **5**, 6826–6831 (2013).
38. J. Li, H. Nomura, H. Miyazaki, C. Adachi, Highly efficient exciplex organic light-emitting diodes incorporating a heptazine derivative as an electron acceptor. *Chem. Commun.* **50**, 6174–6176 (2014).
39. M. Mamada, G. Tian, H. Nakanotani, J. Su, C. Adachi, The Importance of Excited-State Energy Alignment for Efficient Exciplex Systems Based on a Study of Phenylpyridinato Boron Derivatives. *Angew. Chemie Int. Ed.* **57**, 12380–12384 (2018).
40. A. Abragam, M. H. L. Pryce, Theory of the nuclear hyperfine structure of paramagnetic resonance spectra in crystals. *Proc. R. Soc. London. Ser. A. Math. Phys. Sci.* **205**, 135–153 (1951).
41. G. Jeschke, Determination of the nanostructure of polymer materials by electron paramagnetic resonance spectroscopy. *Macromol. Rapid Commun.* **23**, 227–246 (2002).
42. J. A. Weil, J. R. Bolton, *Electron paramagnetic resonance: elementary theory and practical applications* (John Wiley & Sons, 2007).
43. M. Leung, M. A. El-Sayed, Hole burning in the optically detected zero-field spectrum using eedor. *Chem. Phys. Lett.* **16**, 454–459 (1972).
44. J. H. Lee, J. J. Song, M. A. F. Scarparo, M. D. Levenson, Coherent population oscillations and hole burning observed in $\text{Sm}^{+2}:\text{CaF}_2$ using polarization spectroscopy. *Opt. Lett.* (1980), doi:10.1364/ol.5.000196.
45. L. W. Hillman, R. W. Boyd, J. Krasinski, C. R. Stroud, Observation of a spectral hole due to population oscillations in a homogeneously broadened optical absorption line. *Opt. Commun.* **45**, 416–419 (1983).
46. E. Fermi, Über die magnetischen Momente der Atomkerne. *Zeitschrift für Phys.* **60**, 320–333 (1930).
47. R. Kubo, K. Tomita, A General Theory of Magnetic Resonance Absorption. *J. Phys. Soc. Japan.* **9**, 888–919 (1954).
48. M. Brustolon, E. Giamello, *Electron Paramagnetic Resonance* (John Wiley & Sons, Inc., Hoboken, NJ, USA, 2009; <http://doi.wiley.com/10.1002/9780470432235>).
49. L. S. Swanson, Spin dependent recombination in conjugated polymers: an optically detected magnetic resonance study (1991).
50. J. Niklas, K. L. Mardis, B. P. Banks, G. M. Grooms, A. Sperlich, V. Dyakonov, S. Beaupré, M. Leclerc, T. Xu, L. Yu, O. G. Poluektov, Highly-efficient charge separation and polaron delocalization in polymer-fullerene bulk-heterojunctions: A comparative multi-frequency EPR and DFT study. *Phys. Chem. Chem. Phys.* **15**, 9562–9574 (2013).
51. R. Steyrleuthner, Y. Zhang, L. Zhang, F. Kraffert, B. P. Cherniawski, R. Bittl, A. L. Briseno, J. L. Bredas, J. Behrends, Impact of morphology on polaron delocalization in a semicrystalline conjugated polymer. *Phys. Chem. Chem. Phys.* **19**, 3627–3639 (2017).
52. V. Ivády, G. Barcza, G. Thiering, S. Li, H. Hamdi, J. P. Chou, Ö. Legeza, A. Gali, Ab initio theory of the negatively charged boron vacancy qubit in hexagonal boron nitride. *npj Comput. Mater.* **6**, 1–6 (2020).
53. F. Jelezko, T. Gaebel, I. Popa, A. Gruber, J. Wrachtrup, Observation of Coherent Oscillations in a Single Electron Spin. *Phys. Rev. Lett.* **92**, 1–4 (2004).
54. I. I. Vlasov, A. S. Barnard, V. G. Ralchenko, O. I. Lebedev, M. V. Kanyuba, A. V. Saveliev, V. I. Konov, E. Goovaerts, Nanodiamond Photoemitters Based on Strong Narrow-Band Luminescence from Silicon-Vacancy Defects. *Adv. Mater.* **21**, 808–812 (2009).
55. X. Liu, H. Popli, O. Kwon, H. Malissa, X. Pan, B. Park, B. Choi, S. Kim, E. Ehrenfreund, C. Boehme, Z. V. Vardeny, Isotope Effect in the Magneto-Optoelectronic Response of Organic

- Light-Emitting Diodes Based on Donor–Acceptor Exciplexes. *Adv. Mater.* **32**, 2004421 (2020).
56. M. Kivala, T. Stanoeva, T. Michinobu, B. Frank, G. Gescheidt, F. Diederich, One-Electron-Reduced and -Oxidized Stages of Donor-Substituted 1,1,4,4-Tetracyanobuta-1,3-dienes of Different Molecular Architectures. *Chem. - A Eur. J.* **14**, 7638–7647 (2008).
 57. J. Fuchs, G. J. Duffy, W. J. Rowlands, A. Lezama, P. Hannaford, A. M. Akulshin, Electromagnetically induced transparency and absorption due to optical and ground-state coherences in 6Li. *J. Phys. B At. Mol. Opt. Phys.* **40**, 1117–1129 (2007).
 58. A. M. Akulshin, R. Mclean, A. I. Sidorov, P. Hannaford, *ELECTROMAGNETICALLY INDUCED ABSORPTION AND TRANSPARENCY DUE TO LONG-LIVED ZEEMAN COHERENCE* (2009).
 59. E. Baklanov, V. Chebotaev, Resonance Interaction of Unidirectional Waves in Gases. *Sov. J. Exp. Theor. Phys.* **34**, 490 (1972).
 60. N. Bunzmann, D. L. Baird, H. Malissa, S. Weissenseel, C. Boehme, V. Dyakonov, A. Sperlich, Thermal Activation Bottleneck in TADF OLEDs based on m-MTDATA:BPhen. *arXiv*, 1–15 (2020).
 61. W. J. Baker, T. L. Keevers, J. M. Lupton, D. R. McCamey, C. Boehme, Slow Hopping and Spin Dephasing of Coulombically Bound Polaron Pairs in an Organic Semiconductor at Room Temperature. *Phys. Rev. Lett.* **108**, 267601 (2012).
 62. C. G. Yang, E. Ehrenfreund, Z. V. Vardeny, Polaron Spin-Lattice Relaxation Time in π -Conjugated Polymers from Optically Detected Magnetic Resonance. *Phys. Rev. Lett.* **99**, 157401 (2007).
 63. D. R. McCamey, H. A. Seipel, S.-Y. Paik, M. J. Walter, N. J. Borys, J. M. Lupton, C. Boehme, Spin Rabi flopping in the photocurrent of a polymer light-emitting diode. *Nat. Mater.* **7**, 723–728 (2008).
 64. F. Kraffert, R. Steyrlleuthner, C. Meier, R. Bittl, J. Behrends, Transient electrically detected magnetic resonance spectroscopy applied to organic solar cells. *Appl. Phys. Lett.* **107**, 043302 (2015).
 65. E. Hontz, W. Chang, D. N. Congreve, V. Bulović, M. A. Baldo, T. Van Voorhis, The Role of Electron–Hole Separation in Thermally Activated Delayed Fluorescence in Donor–Acceptor Blends. *J. Phys. Chem. C.* **119**, 25591–25597 (2015).
 66. J. Grüne, N. Bunzmann, M. Meinecke, V. Dyakonov, A. Sperlich, Kinetic Modeling of Transient Electroluminescence Reveals TTA as an Efficiency-Limiting Process in Exciplex-Based TADF OLEDs. *J. Phys. Chem. C.* **124**, 25667–25674 (2020).
 67. T. Huang, X. Song, M. Cai, D. Zhang, L. Duan, Improving reverse intersystem crossing in exciplex-forming hosts by introducing heavy atom effect. *Mater. Today Energy.* **21**, 100705 (2021).
 68. Y.-S. Park, K.-H. Kim, J.-J. Kim, Efficient triplet harvesting by fluorescent molecules through exciplexes for high efficiency organic light-emitting diodes. *Appl. Phys. Lett.* **102**, 153306 (2013).
 69. W.-C. Chen, C.-S. Lee, Q.-X. Tong, Blue-emitting organic electrofluorescence materials: progress and prospective. *J. Mater. Chem. C.* **3**, 10957–10963 (2015).
 70. Y. Olivier, B. Yurash, L. Muccioli, G. D’Avino, O. Mikhnenko, J. C. Sancho-García, C. Adachi, T.-Q. Nguyen, D. Beljonne, Nature of the singlet and triplet excitations mediating thermally activated delayed fluorescence. *Phys. Rev. Mater.* **1**, 075602 (2017).
 71. T. Hosokai, H. Matsuzaki, H. Nakanotani, K. Tokumaru, T. Tsutsui, A. Furube, K. Nasu, H. Nomura, M. Yahiro, C. Adachi, Evidence and mechanism of efficient thermally activated delayed fluorescence promoted by delocalized excited states. *Sci. Adv.* **3**, e1603282 (2017).
 72. N. A. Drigo, L. G. Kudriashova, S. Weissenseel, A. Sperlich, A. J. Huckaba, M. K. Nazeeruddin, V. Dyakonov, *J. Phys. Chem. C*, in press, doi:10.1021/acs.jpcc.8b08716.
 73. D. Huertas-Hernando, F. Guinea, A. Brataas, Spin-orbit coupling in curved graphene, fullerenes, nanotubes, and nanotube caps. *Phys. Rev. B.* **74**, 155426 (2006).
 74. H. Liu, J. Wang, A. Chanana, Z. V. Vardeny, Studies of spin transport in fullerene films. *J. Appl. Phys.* **125**, 142908 (2019).
 75. S. Liang, R. Geng, B. Yang, W. Zhao, R. Chandra Subedi, X. Li, X. Han, T. D. Nguyen, Curvature-enhanced Spin-orbit Coupling and Spinterface Effect in Fullerene-based Spin Valves. *Sci. Rep.* **6**, 19461 (2016).
 76. S. Schott, E. R. McNellis, C. B. Nielsen, H.-Y. Chen, S. Watanabe, H. Tanaka, I. McCulloch, K. Takimiya, J. Sinova, H. Siringhaus, Tuning the effective spin-orbit coupling in molecular semiconductors. *Nat. Commun.* **8**, 15200 (2017).
 77. M. Fuchs, J. Schliemann, B. Trauzettel, Ultralong spin decoherence times in graphene quantum dots with a small number of nuclear spins. *Phys. Rev. B.* **88**, 245441 (2013).
 78. F. Kraffert, J. Behrends, Spin-correlated doublet pairs as intermediate states in charge separation processes. *Mol. Phys.* **115**, 2373–2386 (2017).
 79. K. Tvingstedt, O. Malinkiewicz, A. Baumann, C. Deibel, H. J. Snaith, V. Dyakonov, H. J. Bolink,

- Radiative efficiency of lead iodide based perovskite solar cells. *Sci. Rep.* **4**, 6071 (2015).
80. S. Richert, C. E. Tait, C. R. Timmel, Delocalisation of photoexcited triplet states probed by transient EPR and hyperfine spectroscopy. *J. Magn. Reson.* **280**, 103–116 (2017).
81. S. Stoll, A. Schweiger, EasySpin, a comprehensive software package for spectral simulation and analysis in EPR. *J. Magn. Reson.* **178**, 42–55 (2006).

TOC Entry



We disentangle spin-spin interactions and find highly spin-polarized exciplexes in next-generation donor:acceptor TADF OLEDs by magnetic resonance hole burning spectroscopy on operational devices.

125-character teaser

Disentangling spin-spin interactions reveals highly spin-polarized efficiency-limiting exciplexes in next-gen. TADF OLEDs